Eur J Nucl Med Mol Imaging
DOI 10.1007/s00259-016-3594-z

ORIGINAL ARTICLE

Local recurrence of prostate cancer after radical prostatectomy is at risk to be missed in ^{68}Ga-PSMA-11-PET of PET/CT and PET/MRI: comparison with mpMRI integrated in simultaneous PET/MRI

Martin T. Freitag[1,2] · Jan P. Radtke[1,3] · Ali Afshar-Oromieh[4] · Matthias C. Roethke[1] · Boris A. Hadaschik[3] · Martin Gleave[5] · David Bonekamp[1] · Klaus Kopka[6] · Matthias Eder[6] · Thorsten Heusser[7] · Marc Kachelriess[7] · Kathrin Wieczorek[8] · Christos Sachpekidis[2] · Paul Flechsig[4] · Frederik Giesel[4] · Markus Hohenfellner[3] · Uwe Haberkorn[4] · Heinz-Peter Schlemmer[1] · A. Dimitrakopoulou-Strauss[2]

Received: 6 September 2016 / Accepted: 6 December 2016

Abstract

Purpose The positron emission tomography (PET) tracer ^{68}Ga-PSMA-11, targeting the prostate-specific membrane antigen (PSMA), is rapidly excreted into the urinary tract. This leads to significant radioactivity in the bladder, which may limit the PET-detection of local recurrence (LR) of prostate cancer (PC) after radical prostatectomy (RP), developing in close proximity to the bladder. Here, we analyze if there is additional value of multi-parametric magnetic resonance imaging (mpMRI) compared to the ^{68}Ga-PSMA-11-PET-component of PET/CT or PET/MRI to detect LR.

Methods One hundred and nineteen patients with biochemical recurrence after prior RP underwent both hybrid ^{68}Ga-PSMA-11-PET/CT$_{low\text{-}dose}$ (1 h p.i.) and -PET/MRI (2-3 h p.i.) including a mpMRI protocol of the prostatic bed. The comparison of both methods was restricted to the abdomen with focus on LR (McNemar). Bladder-LR distance and recurrence size were measured in axial T2w-TSE. A logistic regression was performed to determine the influence of these variables on detectability in ^{68}Ga-PSMA-11-PET. Standardized-uptake-value (SUV$_{mean}$) quantification of LR was performed.

Results There were 93/119 patients that had at least one pathologic finding. In addition, 18/119 Patients (15.1%) were diagnosed with a LR in mpMRI of PET/MRI but only nine were PET-positive in PET/CT and PET/MRI. This mismatch was statistically significant ($p = 0.004$). Detection of LR using the PET-component was significantly influenced by proximity to the bladder ($p = 0.028$). The PET-pattern of LR-uptake was classified into three types (1): separated from bladder; (2): fuses with bladder, and (3): obliterated by bladder). The size of LRs did not affect PET-detectability ($p = 0.84$), mean size was 1.7 ± 0.69 cm long axis, 1.2 ± 0.46 cm short-axis. SUV$_{mean}$ in nine men was 8.7 ± 3.7 (PET/CT) and 7.0 ± 4.2 (PET/MRI) but could not be quantified in the remaining nine cases (obliterated by bladder).

Conclusion The present study demonstrates additional value of hybrid ^{68}Ga-PSMA-11-PET/MRI by gaining complementary diagnostic information compared to $^{the\ 68}$Ga-PSMA-11-PET/CT$_{low\text{-}dose}$ for patients with LR of PC.

Martin T. Freitag and Jan P. Radtke contributed equally to this work.

✉ Martin T. Freitag
m.freitag@dkfz.de

1 Department of Radiology, German Cancer Research Center, Heidelberg, Germany

2 Clinical Cooperation Unit Nuclear Medicine, German Cancer Research Center, Heidelberg, Germany

3 Department of Urology, University Hospital Heidelberg, Heidelberg, Germany

4 Department of Nuclear Medicine, University Hospital Heidelberg, Heidelberg, Germany

5 The Vancouver Prostate Centre, University of British Columbia, Vancouver, Canada

6 Division of Radiopharmaceutical Chemistry, German Cancer Research Center, Heidelberg, Germany

7 Department of Medical Physics in Radiology, German Cancer Research Center, Heidelberg, Germany

8 Institute of Pathology, University Hospital Heidelberg, Heidelberg, Germany

Published online: 17 December 2016

Keywords ^{68}Ga-PSMA-11 · Local relapse · Local recurrence · PET/MRI · PET/CT · Prostate specific membrane antigen

Abbreviations

ADT	Androgen deprivation therapy
BCR	Biochemical recurrence
CT	Computed tomography
DCE	Dynamic contrast-enhanced imaging
DWI	Diffusion-weighted imaging
GS	Gleason score
LR	Local recurrence
MRI	Magnetic resonance imaging
mpMRI	Multiparametric MRI
PC	Prostate cancer
PET	Positron emission tomography
RP	Radical prostatectomy
RT	Radiotherapy
SUV	Standard uptake value
^{68}Ga	Gallium-68
PSMA	Prostate-specific membrane antigen
^{18}F-FECH	Fluorethylcholine
^{18}F-FDG	2 − ^{18}F-fluoro-2-deoxy-D-glucose

Introduction

Radical prostatectomy (RP) is a standard treatment for localized prostate cancer (PC). Of 100 men treated with RP, approximately 15-30 will develop biochemical recurrence (BCR, defined as prostate-specific antigen ≥ 0.2 ng/ml) [1]. In the situation of BCR, classical manifestations of early recurrent disease after RP include local recurrence (LR) in the prostate fossa as well as lymph node and/or bone metastases. The probability of developing LR is higher in case of positive surgical margins or locally advanced disease (TNM stage ≥ pT3a)[1–4]. Positron emission tomography (PET) targeting the prostate-specific membrane antigen (PSMA) in combination with Gallium-68 labelled PET tracer PSMA-11 (^{68}Ga-PSMA-11-PET) has demonstrated substantial improvement to detect metastatic disease in BCR in combination with magnetic resonance imaging (PET/MRI) and computed tomography (PET/CT) [5–15]. However, the systematic assessment of ^{68}Ga-PSMA-11 for the detection of LR after RP is still unexplored.

LR is defined as a mass arising in the prostate fossa after RP. Especially high accumulation of ^{68}Ga-PSMA-11 within the excreted and concentrated urine in the bladder and consecutive artifacts might be detrimental for detection of LR that evolves with close proximity to the bladder. This assumption is substantiated by previous work demonstrating the same problem for PET-based detection of gynecologic malignancies using 2 − ^{18}F-fluoro-2-deoxy-D-glucose (^{18}F-FDG) which may also develop in close proximity to the bladder [16].

Magnetic resonance imaging (MRI) achieves high tissue contrast in the pelvis that is beneficial for detection of LR [17–21]. Combining multiparametric MRI (mpMRI) and ^{68}Ga-PSMA-11-PET/MRI within simultaneous hybrid PET/MRI might further improve the detectability of LR. We have previously demonstrated inter-method reproducibility between PET/CT and PET/MRI for lymph node and bone metastases of PC [8]. However, the additional or complementary value of ^{68}Ga-PSMA-11 is unclear in the situation of LR. Thus, we compared the diagnostic performance of both PET/MRI and PET/CT to mpMRI (integrated in PET/MRI). We hypothesized that the mpMRI component within PET/MRI provides advantages in the detection rate of LR compared to the ^{68}Ga-PSMA-11-PET-component.

Material and methods

Patients

This retrospective study was approved by the local ethics committee (S-485/2012, S-638/2013) and was conducted in agreement with the Declaration of Helsinki. All patients gave written informed consent. Patients with BCR after RP were considered eligible for comparison if they underwent both ^{68}Ga-PSMA-11-PET/CT and ^{68}Ga-PSMA-11-PET/MRI and if data were entirely available. Patients were excluded if data was not completely matching or incomplete. Out of 145 consecutive patients, 119 (median PSA 1.70 [CI:1.25-2.20] ng/ml) fulfilled the inclusion criteria and underwent PET/CT 1 h p.i. (202 ± 69 MBQ) and PET/MRI 2-3 h p.i. without additional tracer injection between 2013 and 2016 at the Department of Nuclear Medicine at Heidelberg University Medical Center and German Cancer Research Center, DKFZ Heidelberg, Germany. We included a subcohort of patients from previous work [8], in which LR was excluded for systematic comparison. Two different PET/CT scanners (see below) were employed for the current study. Only the abdomen was analyzed for the comparison as the focus of the present work was dedicated to LR.

Imaging

Imaging protocols were partially reported previously [7, 8]. Standardized uptake value (SUV) images were generated as follows: SUV = activity tissue concentration (Bq/ml)/(injected dose (Bq)/body weight (g)).

PET/CT protocol 1 PET/CT acquisition was performed 1 h after injection (p.i.) on a Biograph 6 scanner (Siemens Healthcare, Erlangen, Germany). A low-dose CT scan without contrast enhancement (increment 0.8 mm, soft-tissue kernel, 130 kV, 80 mAs) was acquired followed by a PET acquisition (matrix 164 × 164, 15.5 cm FOV, 4 min/bed position). Random, scatter, and decay correction were applied to the emission data. Data were reconstructed using ordered subsets expectation maximization algorithm (two iterations, eight subsets, Gaussian post-filtering, 5 mm transaxial resolution, full-width at half-maximum). CT data were used for attenuation correction.

PET/CT protocol 2 Prior to the static scan, dynamic images were acquired but not used for the present study. Static images were conducted 1 h p.i. on a time-of-flight compatible PET/CT (Biograph mCT 128S, Siemens Healthcare, Erlangen, Germany) with an axial field of view of 21.6 cm with TruePoint and TrueV, operated in a three-dimensional mode. A low-dose CT (120 kV, 30 mA) from head to the feet was used for attenuation correction of PET-raw data (image matrix of 400 x 400 pixels, iterative reconstruction). An ordered subset expectation maximization algorithm with six iterations and twelve subsets using Gaussian post-filtering 1.5 was used for iterative reconstruction.

PET/MRI protocol Depending on the PET/CT-protocol, the patient was scanned 2 h p.i. (PET/CT protocol 2) or 3 h p.i. (PET/CT protocol 1) at the PET/MRI (Siemens Biograph mMR, Siemens Healthcare, Erlangen, Germany) in the German Cancer Research Center in Heidelberg without additional tracer injection. The Biograph mMR features an axial field of view of 25 cm and a field strength of 3 Tesla. MR-based attenuation correction was performed using the standard two-point Dixon-technique. Data were reconstructed (3-D iterative) using ordered subsets expectation maximization algorithm (three iterations, 21 subsets, Gaussian post-filtering full-width at half-maximum 2). Also, 40% maximum threshold of absolute scatter correction was used in patients with halo artifacts, as previously reported [22].

Parts of the abdominal sequences of PET/MRI protocol were reported previously [8]. This part of the MRI protocol was accompanied by 8 min/bed position PET-acquisition.

1) T1w VIBE native: TE/TR 1.86/4.25 ms, 1.6 × 1.3 × 3 mm, FOV 420 × 275 mm, matrix 320× 256 pixel, GRAPPA 2, distance factor 0, flip angle 10°, slices per slab 72, averages 1, concatenations 1, phase resolution 80%, slice resolution 58%, phase oversampling 10%, slice oversampling 11%, phase partial Fourier 7/8, slice partial Fourier 6/8, bandwidth 450 MHz/pixel, time of acquisition 19 s per slab
2) T2w-haste: TE/TR 91/1000 ms, 1.6 × 1.3 × 5 mm^3, FOV 420 × 315 mm, matrix 320× 259 pixel, GRAPPA 2, flip angle 125°, slices per slab 36, averages 1, concatenations 2, phase resolution 81%, bandwidth 710 MHz/pixel, time of acquisition 42 s per slab
3) Epiplanar diffusion-weighted imaging (DWI): TE/TR 65/2,600 ms, 3.7 × 3 × 5 mm, FOV 380 × 285 mm, matrix 128 × 104 pixel, GRAPPA 2, distance factor 20, flip angle 180°, slices per slab 35, averages 2, concatenations 4, phase partial Fourier 6/8, bandwidth 2442 MHz/pixel, strong SPAIR fat-saturation, b50 and b800 s/mm^2, time of acquisition 3 min 40 s per slab

A dedicated prostate fossa protocol was conducted including T2w TSE axial, coronal, sagittal, diffusion weighted imaging and T1w-dynamic contrast enhanced imaging. This part of the MRI-protocol was accompanied by a 6 min PET-acquisition in order to acquire PET-images that have the same amount of bladder filling as the MRI images allowing perfect alignment and fusion of images.

1) T2w-turbo-spin echo
   a. Axial: TE/TR 146/8000 ms, 0.7 × 0.5 × 3 mm^3, FOV 200 × 100, matrix 384 × 269, phase partial Fourier off, distance factor 10%, averages 2, concatenations 1, flip angle 128°, 28 slices per slab, bandwidth 200 Hz/Px, turbo factor 25, 5 min. 14 sec. time of acquisition.
   b. Sagittal: TE/TR 140/5470 ms, 0.8 × 0.6 × 3 mm^3, FOV 200 × 100, matrix 320 × 256, GRAPPA 2, phase oversampling 75%, distance factor 10%, phase partial Fourier off, averages 2, concatenations 1, 19 slices per slab, bandwidth 191 Hz/Px, turbo factor 20, 2 min. 18 sec. time of acquisition.
2) T2w-BLADE Coronal: TE/TR 108/8110 ms, 0.8 × 0.8 × 3 mm^3, FOV 260 × 260, matrix 320 × 320, averages 1, concatenations 1, 35 slices per slab, bandwidth 300 Hz/Px, turbo factor 23, 3 min. 08 sec. time of acquisition.
3) DWI: TE/TR 86/7500 ms, 2.2 × 2.2 × 3 mm^3, FOV 280 × 210, matrix 128 × 128, phase oversampling 30%, phase partial Fourier 6/8, distance factor 0, flip angle 180°, slices per slab 20, averages 7, concatenations 1, bandwidth 1502 Hz/Px, strong SPAIR fat-saturation, b0, b50 b1000 and b1500 s/mm^2, 9 min. 09 sec. time of acquisition.
4) T1w-dynamic contrast-enhanced (DCE) imaging: TE/TR 2.12/4.52 ms, 5.4 s interval, 50 measurements, 1.6 × 1.6 × 2.0 mm^3, FOV 275 × 400, matrix 176 × 256, GRAPPA 2, slices per slab 40, slice oversampling 10%, flip angle 15°, bandwidth 399 Hz/Px, phase partial Fourier 6/8, slice partial Fourier 6/8, 4 min. 51 sec. time of acquisition.

The total scan time of PET/MRI comprised approximately 1 h 10 min. All patients were asked to void their bladder before PET/CT, as well as before PET/MRI.

Image reading

Two nuclear medicine physicians read and reported the PET/CT images during clinical routine (one senior: U.H., A.D.S., or F.G. and one resident: P.F. or C.S.). PET/MRI were read by four radiologists (one senior: H.P.S., M.C.R., D.B. or M.T.F..; one resident) during clinical routine. For the PET-component of the PET/MRI, a senior nuclear medicine physician from the PET/CT reading team was consulted. The complete data was read for consistency (M.T.F.). All patients were read in consensus of either PET/CT or PET/MRI, respectively, but final reports were treated separately.

Histopathological and biochemical confirmation of LR

Subsequent treatment was performed under guidance of an experienced senior urologist (B.A.H., M.H. or M.G.) using the synopsis of both PET/CT and PET/MRI reports. If PET/MRI and PET/CT differed in their interpretation of LR, histopathological evidence was searched only in uncertain cases in accordance with guideline recommendations [1, 23]. Otherwise, LRs were validated by follow-up imaging and/or significant PSA decrease after salvage-therapy. Follow-up imaging modalities included ^{68}Ga-PSMA-11-PET, mpMRI, contrast-enhanced CT or endorectal ultrasound. If follow-up imaging demonstrated decrease in lesion size and if PSA levels decreased after salvage treatment, LR was assumed to be confirmed. Metastases, if present, were noted and reported in the results section, but were neglected for inter-method comparison as this topic has been investigated earlier [8, 24].

Image evaluation

Standard windowing was [0-2.5-5 SUV] for all patients. SUV_{mean} of LR was measured. A 2-D-region-of-interest was chosen over thresholded 3-D-isocontour, because the automatic algorithm would have led to segmentation of the bladder close to LR and, thus, failed to produce appropriate ROIs for SUV measurements.

The shortest distance between the most distant part of recurrence and the inner bladder wall was measured in axial T2w TSE in mm (Fig. 1). The mean size was measured by using the long and short axis. The area (long x short axis) was noted in mm^2.

For all patients, the presence of surgical clips was evaluated based on the CT scans. Only clips in the prostate bed were counted. Surgical clips along the parailiacal axis due to lymphadenectomy were neglected because they usually do not pose a problem for prostate bed assessment. For patients with LR in mpMRI, impact of artifacts resulting from surgical clips was noted per MRI sequence

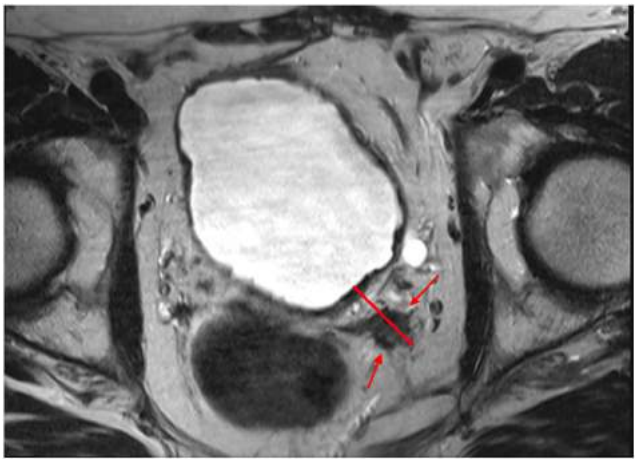

Fig. 1 Determination of the distance between bladder and recurrence in axial T2w-TSE. The most distant point of recurrence (red arrows) and the shortest distance to the bladder mucosa was measured (red line). In this example the distance is 2.5 cm

(0-3 scale): 0 no surgical clips; 1: clips present but not detrimental for image assessment; 2: susceptibility artifacts from clips slightly influence the depiction of pathology; and 3: susceptibility artifacts from clips heavily influence the depiction of pathology.

The mpMRI protocol was interpreted taking the synopsis of T2w-TSE/DWI and T1w-DCE.

Statistical analysis

All statistical tests were performed using SPSS (IBM, Armonk, USA). First, McNemar's test was performed to assess whether there was a significant difference in LR detection between PET/CT and PET/MRI. To determine the influence of bladder-recurrence distance and size of the recurrence on detectability in PET, a multiple logistic regression model was used, in which PET-positivity (yes/no) was the dependent nominal variable and the distance in mm and the size of the lesion in mm^2 the independent variables. Bootstrapping was used based on 1000 samples. All tests were performed 2-sided with a significance level of 5%.

Results

Patient demographics and LR confirmation of PET/CT findings

Twenty-six patients (21.8%) did not reveal any pathology on PET-imaging while 93 showed PSMA-positive lesions. Within the cohort, 18 men demonstrated LR in PET/MRI (Table 1), while LR was detected by PSMA-PET/CT in nine patients (Table 2). The same nine PSMA-PET/CT-positive patients were also PSMA-PET/MRI positive.

Table 1 Patient characteristics with LR ($n = 18$)

Patient characteristics	Number of patients MBq of ^{68}Ga-PSMA-11 applied	18 217.11 ± 52.84
Laboratory and histopathological results	PSA values (ng/ml)	Median 3.25 [CI:1.20-5.23]*
	Gleason score distribution	GSC 5 ($n = 1$)
		GSC 6 ($n = 3$)
		GSC 7 ($n = 9$)
		GSC 8 ($n = 1$)
		GSC 9 ($n = 2$)
		N/A $n = 2$
Previous salvage-treatment	no treatment	5
	RT only	9
	ADT only	3
	ADT + RT	1

RT: Radiotherapy of the prostate bed; ADT: androgen deprivation therapy *95% confidence interval for the median

The LR mismatch between PET of PET/MRI ($n = 9$) and PET/C T ($n = 9$) and mpMRI ($n = 18$) was statistically significantly different ($p < 0.004$). There was no PSMA-11-PET-positive/MRI-negative LR.

Seven out of 18 patients underwent subsequent biopsy confirming LR. In 11 patients, the mpMRI and/or PET-detected LR was validated by PSA-decrease after local salvage-treatment and subsequent follow-up PSA measurements.

Image evaluation

Three different types of LRs were noted in PSMA-11-PET of both PET/CT and PET/MRI (Fig. 2, 3, 4, and 5). Between 2.2 ± 0.4 cm LR was depicted as an independent PET-uptake and visible in the PET of PET/MRI and PET/CT (type 1 recurrence). There was some overlap of bladder-LR distance (2 ± 0.4 cm) leading to a fusion of lesion and bladder signal in PET of PET/MRI and PET/CT (type 2 recurrence) compared to the first type. However, re-windowing the attenuation-corrected PET-images in type 2 LR helped to discriminate areas with different uptake, e.g., the bladder and the adjacent pathology. Type 3 (1.3 ± 0.5 cm distance) was defined by complete PET-negativity by the obliterating bladder signal whereas mpMRI detected LR. The SUV of 9 LRs could be quantified (PET/CT 8.7 ± 3.7 and PET/MRI 7.0 ± 4.2) in the same patients. There was no significant different pattern in SUV uptake between 1 h p.i. in PET/CT and 3 h p.i. in PET/MRI. Consequently, the remaining PET-negative LRs ($n = 9$) could not be quantified due to the bladder signal outshining the recurrence.

Mean diameter of all LRs was 1.7 ± 0.69 cm in long axis and 1.2 ± 0.45 cm in short-axis. Mean diameter of PET-negative but MRI-positive LRs ($n = 9$) was similar (1.74 ± 0.52 cm long axis, 1.09 ± 0.32 cm short axis). In the CT-based analysis, 68.1% (81/119) of patients enrolled in the study showed at least one surgical clip in the prostate bed. In addition, 31.9% had zero (38/119), 4.2% had one (5/119), 16.8% had two (20/119) and 47.1% (56/119) had three or more surgical clips.

Table 2 LR detection rates depending on the modality

	Prostate-bed mpMRI	PET of PET/CT	PET of PET/MRI
Men with LR	18	9	9
Frequency within cohort ($n = 119$)	15.1%	7.6%	7.6%
SUV	-	8.7 ± 3.7	7.0 ± 4.2
*Artifact impact of surgical clips (0-3; mean + stdev)	DWI 1.1 ± 1.17	-	-
	T1w-DCE 0.3 ± 0.66		
	T2w TSE 0.21 ± 0.63		

Between PET/CT and PET/MRI, there was a mismatch of nine LRs. Subsequent treatment was adjusted to mpMRI. Ten LRs between both PET/CT and PET/MRI correspond to the same patients. The nine LRs detected by PET/CT and PET/MRI are all included in the 18 LRs detected by the mpMRI of the prostate bed.

* Artifact impact: 0 no surgical clips; 1: clips present but not detrimental for image assessment; 2: susceptibility artifacts from clips slightly influence the depiction of pathology; 3: susceptibility artifacts from clips heavily influence the depiction of pathology

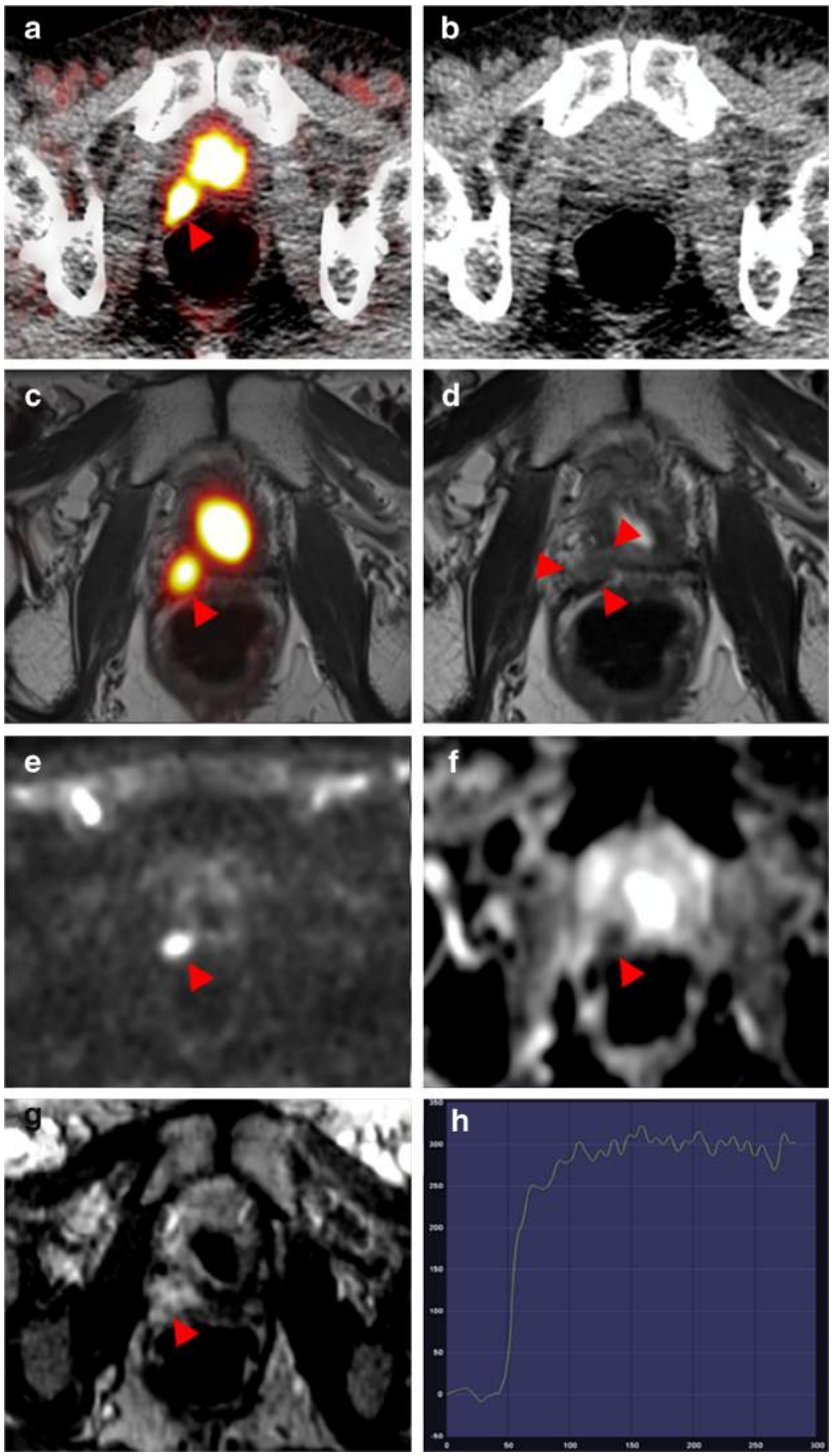

Fig. 2 : Patient example of a LR with distance from the bladder. A 76-year-old patient with history of radical prostatectomy (Gleason 7, determined by surgery) presenting with PSA 2.57 ng/ml. The images show the comparison of ^{68}Ga-PSMA-PET/CT (**a**,**b**) and multiparametric ^{68}Ga-PSMA-PET/MRI of the prostate bed including T2w-PET-fusion (**c**), T2w axial (**d**), DWI at b = 1500 s/mm^2 (**e**), ADC-map mm^2/s (**f**), T1w-dynamic contrast-enhanced sequence (**g**) with time-dependent curve (**h**). x-axis in (**h**) corresponds to time in seconds, y-axis relative signal. This example demonstrates PET-positive LR with sufficient distance from the bladder. Note that low-dose CT (**b**) does not have sufficient spatial resolution and contrast to depict the recurrence. Here, the mpMRI-sequences serve to confirm the diagnosis already assumed by PET and help differentiating it from the signal of the ureter

For MRI, on a scale from 0 (no artifact) to 3 (large artifact) as described in methods, DWI was most prone to surgical clips (1.1 ± 1.17), followed by T1w–DCE (0.3 ± 0.66) and T2w-TSE (0.21 ± 0.54). Using multiple logistic regression analysis, Cox & Snell $R^2 = 0.41$, Nagelkerke's $R^2 = 0.55$, Table 3), the bladder-to-LR distance, measured in mm in T2w-TSE, was identified as a statistically significant predictor of PET-positivity ($p = 0.028$). In contrast, the LR size (long axis x short axis) was not a significant parameter of accurate LR detection using PET ($p = 0.84$). Table 4 demonstrates the coherence between LR distance and the observed PET pattern.

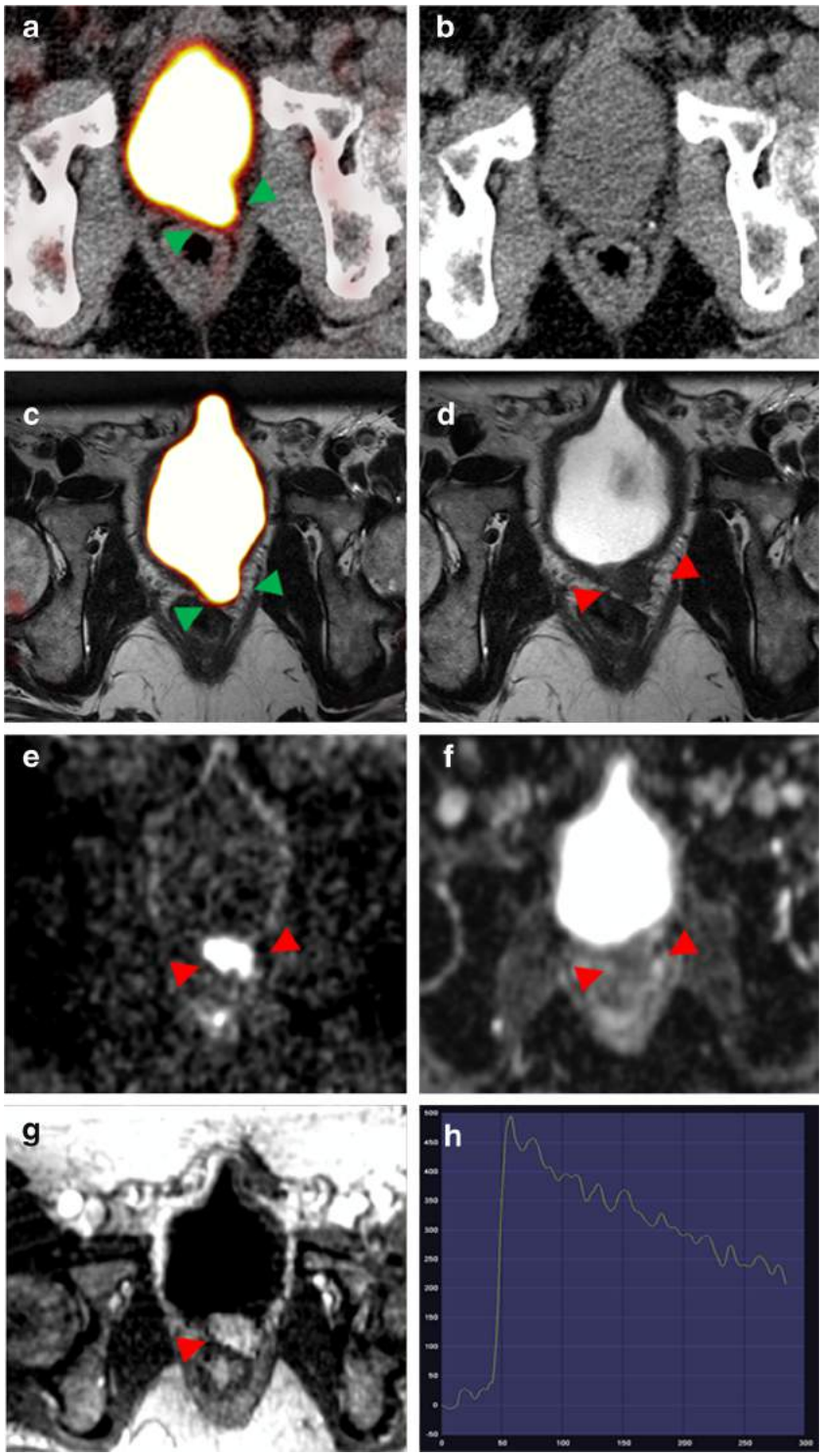

Fig. 3 Patient example of a LR close to the bladder. 63-year-old patient presenting after radical prostatectomy with elevated PSA levels (15 ng/ml) indicating biochemical recurrence. This example demonstrates ^{68}Ga-PSMA-11-PET-positive LR where the corresponding uptake fuses with the signal of the bladder. Parts of the recurrence infiltrate the bladder wall. Thus, detection is impeded in PET and MRI and helps to confirm the diagnosis. The images demonstrate the comparison of ^{68}Ga-PSMA-11-PET/CT (**a**,**b**) and multiparametric ^{68}Ga-PSMA-11-PET/MRI of the prostate bed including T2w-PET-fusion (**c**), T2w axial (**d**), DWI at b = 1500 s/mm^2 (**e**), ADC-map mm^2/s (**f**), T1w-dynamic contrast-enhanced sequence (**g**) with time-dependent curve (**h**). x-axis in (**h**) corresponds to time in seconds, y-axis relative signal. Note that low-dose CT (**b**) does not have sufficient spatial resolution and contrast to depict the recurrence

Discussion

MpMRI of the prostate bed is one of the best available imaging tools for LR assessment after RP [1, 17–19, 21, 25–28]. In addition, recent reports demonstrated potential for LR detection using fluorethylcholine (^{18}F-FECH-PET) [29, 30]. However, inferiority for ^{18}F-FECH-PET compared to ^{68}Ga-PSMA-11-PET was demonstrated for imaging of recurrent PC due to the excellent diagnostic accuracy of ^{68}Ga-PSMA-11 for PC-related tissue [15, 31, 32]. Therefore, ^{68}Ga-PSMA-11-PET could have potential advantages for detection of metastatic foci and possibly LR. However, in the current study 50% of LR was not detected by ^{68}Ga-PSMA-11-PET, neither in the PET of PET/CT (1 h), nor in the PET of PET/MRI (3 h

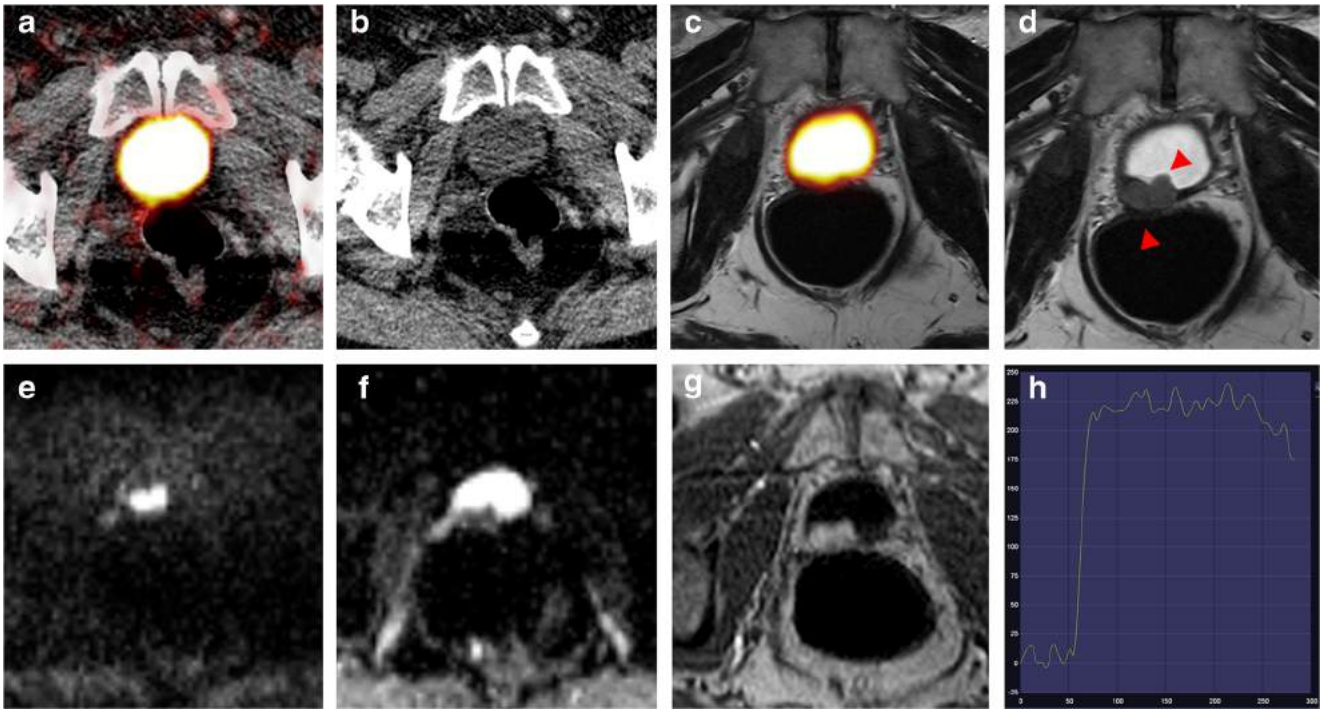

Fig. 4 Patient example of a LR completely superimposed by bladder radioactivity. A 66-year-old patient after radical prostatectomy (Gleason 8) presenting with biochemical recurrence (PSA 1.2 ng/ml). Example of histologically confirmed (biopsy) PET-invisible LR. PET/CT (**a**) was negative, low-dose CT was negative (**a**,**b**). PET of PET/MRI was negative (**c**). mpMRI of the prostate bed demonstrates bladder-wall infiltrating LR (red arrow heads) in morphological T2w TSE (**d**) demonstrating rapid enhancement in T1w-DCE (e,**f**) accompanied by late wash-out phenomenon. The x-axis in (**e**) corresponds to time in seconds and the y-axis represents signal intensity in arbitrary units

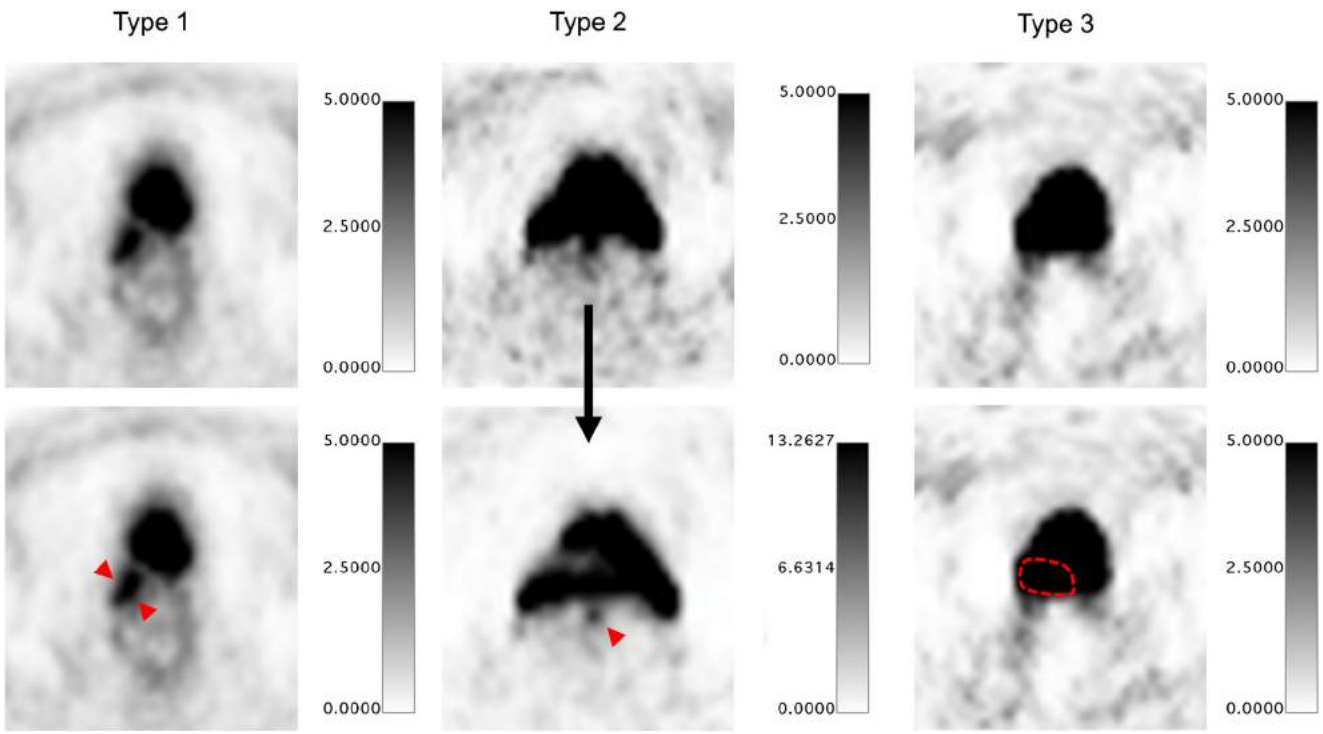

Fig. 5 Classification of LRs depending on proximity to the bladder. Classification of LRs depending on PET-positivity. Type 1: recurrence (red arrow heads) is depicted as a separate signal in standard windowing [0 - 2.5 - 5 SUV]. Type 2: Fusion of PET-positive recurrence (red arrow head) and bladder resulting from close proximity. Use re-windowing to gain better information on different activity distributions. Type 3: Recurrence (red lines) infiltrates bladder wall. Thus, LR is not detectable using ^{68}Ga-PSMA-11 PET - > MRI needed for exclusion

Table 3 Statistical coherence of bladder-recurrence distance and detectability in ^{68}Ga-PSMA-11-PET

	Regression Coefficient B	StdError	Wald	p-value	Odds (exp(B))
Recurrence distance	3.34 [1.26 – 291.20]	1.52	4.85	$p = 0.028$	28.11 [1.44 – 547.44]
Recurrence size	0.001 [-0.50 - 0.06]	0.004	0.043	$p = 0.836$	1 [0.99 – 1.01]

Decrease in bladder-wall-recurrence distance significantly predicts ^{68} Ga-PSMA-PET-negativity whereas the size of recurrence does not significantly influence the PET-based visibility. [95% bootstrap confidence intervals based on 1000 samples]. See Table 4 for the relationship of distance in cm and visualization.

p.i.). This underdetection is explained by the interfering accumulation of ^{68}Ga-PSMA-11-PET within a 'hot' bladder, resulting from a high tracer concentration in the urine. Despite all patients were asked to void their bladder prior to both PET scans, respectively, the accumulation of ^{68}Ga-PSMA-11-PET within the bladder was obliterating potential uptake of LR resulting in a false-negative diagnosis. We could demonstrate that the detection of LR in ^{68}Ga-PSMA-11-PET is statistically dependent on the bladder-LR-distance that could be reliably determined by mpMRI. With decreasing bladder-recurrence distance, as defined in the methods section, the detection of LR is impeded in ^{68}Ga-PSMA-PET ($p = 0.028$). A simple imaging-based classification for clinical routine is proposed that recognizes this pitfall (Figs. 2, 3, 4 and 5, Table 4). Since LR may evolve in close proximity to the bladder ($n = 9$) infiltrating the serosa and the muscular layers, it may be completely masked in the PET by the bladder signal and, hence, remain undetected. The good performance of mpMRI in the present study is straightforwardly explained as the bladder does not confound in mpMRI as follows (see Figs. 2, 3 and 4 for examples): (1) T2w-TSE: the bladder shows water-equivalent signal but recurrence is depicted with low signal, (2) DWI: at high b-values, the bladder is hypointense but recurrence is hyperintense, and (3) T1w-DCE: no signal within bladder in early phase while recurrence shows accumulation of contrast medium.

To improve the ^{68}Ga-PSMA-11-PET-performance for detection of LR, the intravenous application of furosemide in combination with infusion of physiological saline solution can be discussed to decrease the filling of the bladder by increasing the total voiding volume of the patient and to reduce the radioactivity of the bladder. However, images that have been reported from other groups using furosemide for ^{68}Ga-PSMA-11-PET scans reveal a similar pattern of the "hot" bladder [12]. It remains unclear, whether the detection rate of ^{68}Ga-PSMA-11-PET will match mpMRI after application of furosemide. As furosemide forces the patient to urinate in the PET/MRI scanner potentially leading to radioactive contamination, the workflow has to be perfectly optimized for this purpose. Placement of an indwelling transurethral bladder catheter prior to the PET-scan should be discussed with respect to radiation protection and patient compliance to reduce both, potential contamination and bladder filling. Furthermore, late imaging (3 h p.i.) in combination with hydration/furosemide may help to identify unclear lesions by using the pharmacokinetics of the tracer. Our study provides evidence, that without such potential improvements, the LR detection rate of ^{68}Ga-PSMA-11-PET is reduced compared to mpMRI. According to these results and since no guidelines exist towards PSMA-imaging, morphological "backup"-imaging of the prostate bed by mpMRI or at least contrast-enhanced CT, if no MRI is available, can help to reduce false-negative rate of PET/CT. Concluding from our results, studies reporting diagnostic accuracy in biochemical recurrence of PC using ^{68}Ga-PSMA-11-PET/CT$_{low\text{-}dose}$ scan potentially underestimate the detection rate of LRs. Especially in patients with a completely

Table 4 Dependency of bladder-recurrence distance and ^{68}Ga-PSMA-11-PET-detectability classified into three subtypes (see also Fig. 5)

Type	Number of patients	Bladder-recurrence distance	Definition	Figure example
1	5 of 18	2.2 ± 0.4 cm	The LR is visualized as an independent lesion from the bladder signal in ^{68}Ga-PSMA-11-PET	Figure 2
2	4 of 18	2.0 ± 0.4 cm	The LR is closely located to the bladder signal and thus visualized as a fusion between both uptakes in ^{68}Ga-PSMA-11-PET	Figure 3
3	9 of 18	1.3 ± 0.5 cm	The LR is invisible in ^{68}Ga-PSMA-11-PET being superimposed by the bladder signal	Figure 4

As determined by logistic regression (Table 3), the bladder-recurrence distance is a predictor for PET-positivity or -negativity ($p = 0.028$). With decreasing bladder-recurrence distance, the detection of LR is impeded in ^{68} Ga-PSMA-11-PET. This classification is based on standard windowing [0 - 2.5 - 5 SUV].

negative ^{68}Ga-PSMA-11-PET/CT$_{low-dose}$ presenting with BCR, mpMRI of the prostate-bed should be considered to gain a maximum in patient security.

Future studies are needed to compare the benefit of furosemide and bladder catheterization to potentially improve the PET-performance for LR detection. Furthermore, more recent tracer developments may show different patterns of radioactivity in the bladder potentially facilitating LR detection [33]. The combination of both ^{68}Ga-PSMA-11-PET and mpMRI, conducted in a simultaneous fashion at a hybrid PET/MRI scanner, combines the already established excellent capability of ^{68}Ga-PSMA-11-PET for distant metastases [10, 11, 34] together with the high spatial resolution and functional T1w-DCE information of mpMRI necessary for detection of LRs [1] as demonstrated in the present study. We cannot exclude that MRI-negative/^{68}Ga-PSMA-11-PET-positive LRs exist. However, they would be also covered by the PET-component of PET/MRI substantiating the complementary value of hybrid ^{68}Ga-PSMA-11-PET/MRI for patients with BCR. In line with this assumption, such benefit of complementary information of hybrid ^{68}Ga-PSMA-11-PET/MRI has previously been shown for primary PC [35].

The present study is subject to several limitations. Firstly, we cannot provide diagnostic accuracy parameters, because patients without BCR and men without any suspicious lesions did not undergo biopsy or specific salvage-radiotherapy of the prostate fossa. Secondly, we acknowledge that not every LR was confirmed by histopathology. However, if LR is obvious based on imaging and BCR is present, routinely histopathologic confirmation is not necessary according to current guidelines [23]. Even with guidance, the sensitivity of anastomotic biopsies remains poor (40-71% for PSA levels > 1 ng/mL and 14-45% for PSA levels < 1 ng/mL) [1, 36]. This approach is also accepted, if distant metastases, e.g., lymph nodes or systematic disease occur [23]. Therefore, patients without histological conformation were validated by PSA decrease after subsequent therapy and/or imaging follow-up. A third limitation addresses the time difference between PET-acquisitions between PET/CT (1 h p.i.) and PET/MRI (3 h p.i.). Here, the detection rate in the PET-component was equal between both examinations ($n = 9$). Therefore, this bias of LR detection rate can be very likely excluded. We did not observe a significant benefit of late imaging for LR in those nine patients in whom LR was detectable. SUV_{mean} was slightly lower but similar (PET/CT 8.7 ± 3.7 and PET/MRI 7.0 ± 4.2). The benefit of late imaging should be assessed anew after using a dedicated protocol for reducing bladder radioactivity. Fourthly, "halo" artifacts, as reported previously, evolving in the bladder region may be influencing image quality and diagnosis [24]. To reduce these artifacts, all patients were asked to void their bladder before the PET/CT scan as well before the PET/MRI scan. Furthermore, we used the recently reported absolute scatter correction employing a maximum scatter fraction threshold of 40% that helps producing artifact-free images [22]. Fifthly, we did not analyze the role of ^{68}Ga-PSMA-11-PET/CT using contrast-enhanced CT. However, even with contrast-agent, the spatial resolution and soft-tissue contrast of CT within the prostate bed is decreased compared to mpMRI and the sensitivity of contrast-enhanced CT for LR detection is low [1]. Sixthly, mpMRI can be influenced from susceptibility artifacts due to surgical clips. In addition, 68.1% of patients demonstrated surgical clips in the prostate bed based on the CT scans. In the majority of patients with LR, these artifacts were tolerable in mpMRI and did not lead to significant decreased image quality. Artifacts are typically most prominent in gradient-echo based sequences and decrease in turbo-spin echo sequences. Both sequence types are included in the prostate mpMRI protocol. Lastly, the present study focused on LR, comparing only the pelvis. However, our previous PET/MRI study demonstrated PSMA-imaging from the thorax to the pelvis [8]. Extending the field-of-view to cover the whole-body, but maintaining the possibility for high-resolution prostate-bed imaging, is desirable with regard to acceptable, cost-efficient acquisition times. Because LR is a common pathology in BCR of PC that needs to be excluded, mpMRI of the prostate bed should be considered in hybrid ^{68}Ga-PSMA-11-PET/MRI.

Conclusion

This study demonstrates additional benefit of ^{68}Ga-PSMA-11-PET/MRI compared to ^{68}Ga-PSMA-11-PET/CT for patients with BCR to detect LR of PC due to complementary diagnostic information. LR of PC with close proximity and/or infiltration of the bladder occurs frequently and is at risk to be missed in ^{68}Ga-PSMA-11-PET as the radioactivity in the bladder may obliterate the pathology and, thus, impede accurate recurrence assessment if no remedy is undertaken to significantly reduce bladder radioactivity. The ^{68}Ga-PSMA-11-PET/MRI provides 'backup' or 'confirmation' imaging using mpMRI for PET-negative LRs, e.g., such as those obliterated by bladder background.

Acknowledgements We would like to express our gratitude to Dr. Stefan Kegel and the support of our technicians Regula Gnirs, Heike Streib-Retzbach, Julia Schliebus, Cora Weyrich, and Rene Hertel for their excellent support.

Compliance with ethical standards

Funding There was no funding for this study.

Conflicts of interest Heinz-Peter Schlemmer, Ali Afshar-Oromieh and Matthias C. Roethke have received honoraria from Siemens Healthcare for educational sessions. The other authors report no conflict of interest.

Informed consent All procedures performed in studies involving human participants were in accordance with the ethical standards of the institutional and/or national research committee and with the 1964 Helsinki Declaration and its later amendments or comparable ethical standards. Informed consent was obtained from all individual participants included in the study.

References

1. Mottet N, Bellmunt J, Briers E, Bolla M, Cornford P, De Santis M, et al. Guidelines on prostate cancer. Eur Assoc Urol. 2016;53:68–80.
2. Stephenson AJ, Scardino PT, Eastham JA, Bianco FJ, Dotan ZA, Fearn PA, et al. Preoperative nomogram predicting the 10-year probability of prostate cancer recurrence after radical prostatectomy. J Natl Cancer Inst. 2006;98:715–7.
3. Fossati N, Karnes RJ, Boorjian SA, Moschini M, Morlacco A, Bossi A, et al. Long-term Impact of Adjuvant Versus Early Salvage Radiation Therapy in pT3N0 Prostate Cancer Patients Treated with Radical Prostatectomy : Results from a Multi-institutional Series. Eur. Urol. Eur Assoc Urol; 2016;1–8.
4. Pfitzenmaier J, Pahernik S, Tremmel T, Haferkamp A, Buse S, Hohenfellner M. Positive surgical margins after radical prostatectomy: do they have an impact on biochemical or clinical progression? BJU Int. 2008;102:1413–8.
5. Eder M, Schäfer M, Bauder-Wüst U, Hull WE, Wängler C, Mier W, et al. 68Ga-complex lipophilicity and the targeting property of a urea-based PSMA inhibitor for PET imaging. Bioconjug Chem. 2012;23:688–97.
6. Afshar-Oromieh A, Haberkorn U, Eder M, Eisenhut M, Zechmann C. [68Ga]Gallium-labelled PSMA ligand as superior PET tracer for the diagnosis of prostate cancer: comparison with 18F-FECH. Eur J Nucl Med Mol Imaging. 2012;39:1085–6.
7. Sachpekidis C, Kopka K, Eder M, Hadaschik BA, Freitag MT, Pan L, et al. 68Ga-PSMA-11 dynamic PET/CT imaging in primary prostate cancer. Clin Nucl Med. 2016;41:e473–9.
8. Freitag MT, Radtke JP, Hadaschik BA, Kopp-Schneider A, Eder M, Kopka K, et al. Comparison of hybrid 68Ga-PSMA PET/MRI and 68Ga-PSMA PET/CT in the evaluation of lymph node and bone metastases of prostate cancer. Eur J Nucl Med Mol Imaging. 2015;43:70–83.
9. Afshar-Oromieh A, Malcher A, Eder M, Eisenhut M, Linhart HG, Hadaschik BA, et al. PET imaging with a [68Ga]gallium-labelled PSMA ligand for the diagnosis of prostate cancer: biodistribution in humans and first evaluation of tumour lesions. Eur J Nucl Med Mol Imaging. 2013;40:486–95.
10. Afshar-Oromieh A, Avtzi E, Giesel FL, Holland-Letz T, Linhart HG, Eder M, et al. The diagnostic value of PET/CT imaging with the 68Ga-labelled PSMA ligand HBED-CC in the diagnosis of recurrent prostate cancer. Eur. J. Nucl. Med. Mol. Imaging. 2014;1–13.
11. Eiber M, Maurer T, Souvatzoglou M, Beer AJ, Ruffani A, Haller B, et al. Evaluation of hybrid 68Ga-PSMA-ligand PET/CT in 248 patients with biochemical recurrence after radical prostatectomy. J Nucl Med. 2015;56:668–74.
12. Rauscher I, Maurer T, Fendler WP, Sommer WH, Schwaiger M, Eiber M. (68)Ga-PSMA ligand PET/CT in patients with prostate cancer: How we review and report. Cancer Imaging Off Publ Int Cancer Imaging Soc. 2016;16:14.
13. Rauscher I, Maurer T, Beer AJ, Graner F-P, Haller B, Weirich G, et al. Value of 68Ga-PSMA HBED-CC PET for the assessment of lymph node metastases in prostate cancer patients with biochemical recurrence: comparison with histopathology after salvage lymphadenectomy. J. Nucl. Med. Off. Publ. Soc. Nucl. Med. 2016
14. Perera M, Papa N, Christidis D, Wetherell D, Hofman MS, Murphy DG, et al. Sensitivity, Specificity, and Predictors of Positive 68Ga–Prostate-specific Membrane Antigen Positron Emission Tomography in Advanced Prostate Cancer: A Systematic Review and Meta-analysis. Eur. Urol. [Internet]. 2016 [cited 2016 Jun 29]; Available from: Perera M, Papa N, Christidis D, Wetherell D, Hofman MS, Murphy DG, et al. Sensitivity, Specificity, and Predictors of Positive 68Ga–Prostate-specific Membrane Antigen Positron Emission Tomography in Advanced Prostate Cancer: A Systematic Review and Meta-analysis. Eur. Urol. [Internet]. 2016 [cited 2016 Jun 29]; Available from: http://linkinghub.elsevier.com/retrieve/pii/S0302283816302937
15. Afshar-Oromieh A, Zechmann CM, Malcher A, Eder M, Eisenhut M, Linhart HG, et al. Comparison of PET imaging with a 68Ga-labelled PSMA ligand and 18F-choline-based PET/CT for the diagnosis of recurrent prostate cancer. Eur J Nucl Med Mol Imaging. 2014;41:11–20.
16. Roman-Jimenez G, Crevoisier RD, Leseur J, Devillers A, Ospina JD, Simon A, et al. Detection of bladder metabolic artifacts in 18F-FDG PET imaging. Comput Biol Med. 2016;71:77–85.
17. Linder BJ, Kawashima A, Woodrum DA, Tollefson MK, Karnes J, Davis BJ, et al. Early localization of recurrent prostate cancer after prostatectomy by endorectal coil magnetic resonance imaging. Can J Urol. 2014;21:7283–9.
18. Barchetti F, Panebianco V. Multiparametric MRI for Recurrent Prostate Cancer Post Radical Prostatectomy and Postradiation Therapy. BioMed Res Int. 2014;2014:1–23.
19. Panebianco V, Barchetti F, Sciarra A, Musio D, Forte V, Gentile V, et al. Prostate cancer recurrence after radical prostatectomy: the role of 3-T diffusion imaging in multi-parametric magnetic resonance imaging. Eur Radiol. 2013;23:1745–52.
20. Park JJ, Kim CK, Park SY, Park BK, Lee HM, Cho SW. Prostate Cancer: Role of Pretreatment Multiparametric 3-T MRI in Predicting Biochemical Recurrence After Radical Prostatectomy. Am J Roentgenol. 2014;202:W459–65.
21. Kitajima K, Hartman RP, Froemming AT, Hagen CE, Takahashi N, Kawashima A. Detection of Local Recurrence of Prostate Cancer After Radical Prostatectomy Using Endorectal Coil MRI at 3 T: Addition of DWI and Dynamic Contrast Enhancement to T2-Weighted MRI. Am J Roentgenol. 2015;205:807–16.
22. Heusser T, Mann P, Schäfer M, Dimitrakopoulou-Strauss A, Kachelrieß M, Schlemmer H-P, et al. The Halo-Artifact in 68Ga-PSMA-PET/MRI: Studies Using Phantom and Clinical Data. 5th PSMR Conf. PETMR SPECTMR. 2016.
23. Heidenreich A, Bastian PJ, Bellmunt J, Bolla M, Joniau S, van der Kwast T, et al. EAU guidelines on prostate cancer. Part II: Treatment of advanced, relapsing, and castration-resistant prostate cancer. Eur Urol. 2014;65:467–79.
24. Afshar-Oromieh A, Haberkorn U, Schlemmer HP, Fenchel M, Eder M, Eisenhut M, et al. Comparison of PET/CT and PET/MRI hybrid systems using a 68Ga-labelled PSMA ligand for the diagnosis of recurrent prostate cancer: initial experience. Eur J Nucl Med Mol Imaging. 2014;41:887–97.
25. Roy C, Foudi F, Charton J, Jung M, Lang H, Saussine C, et al. Comparative Sensitivities of Functional MRI Sequences in Detection of Local Recurrence of Prostate Carcinoma After Radical Prostatectomy or External-Beam Radiotherapy. Am J Roentgenol. 2013;200:W361–8.
26. Carbone SF, Pirtoli L, Ricci V, Carfagno T, Tini P, La Penna A, et al. Diffusion-Weighted Magnetic Resonance Diagnosis of Local Recurrences of Prostate Cancer after Radical Prostatectomy: Preliminary Evaluation on Twenty-Seven Cases. BioMed Res Int. 2014;2014:1–8.

27. Lopes Dias J, Lucas R, Magalhães Pina J, João R, Costa NV, Leal C, et al. Post-treated prostate cancer: normal findings and signs of local relapse on multiparametric magnetic resonance imaging. Abdom Imaging. 2015;40:2814–38.
28. Couñago F, del Cerro E, Recio M, Díaz AA, Marcos FJ, Cerezo L, et al. Role of 3T multiparametric magnetic resonance imaging without endorectal coil in the detection of local recurrent prostate cancer after radical prostatectomy: the radiation oncology point of view. Scand J Urol. 2015;49:360–5.
29. Evangelista L, Cimitan M, Hodolič M, Baseric T, Fettich J, Borsatti E. The ability of 18F-choline PET/CT to identify local recurrence of prostate cancer. Abdom Imaging. 2015;40:3230–7.
30. Paparo F, Piccardo A, Bacigalupo L, Romagnoli A, Piccazzo R, Monticone M, et al. Value of bimodal 18F-choline-PET/MRI and trimodal 18F-choline-PET/MRI/TRUS for the assessment of prostate cancer recurrence after radiation therapy and radical prostatectomy. Abdom Imaging. 2015;40:1772–87.
31. Bluemel C, Krebs M, Polat B, Linke F, Eiber M, Samnick S, et al. 68Ga-PSMA-PET/CT in Patients With Biochemical Prostate Cancer Recurrence and Negative 18F-Choline-PET/CT. Clin Nucl Med. 2016;41:515–21.
32. Morigi JJ, Stricker PD, van Leeuwen PJ, Tang R, Ho B, Nguyen Q, et al. Prospective Comparison of 18F-Fluoromethylcholine Versus 68Ga-PSMA PET/CT in Prostate Cancer Patients Who Have Rising PSA After Curative Treatment and Are Being Considered for Targeted Therapy. J Nucl Med. 2015;56:1185–90.
33. Giesel FL, Cardinale J, Schäfer M, Neels O, Benešová M, Mier W, et al. (18)F-Labelled PSMA-1007 shows similarity in structure, biodistribution and tumour uptake to the theragnostic compound PSMA-617. Eur J Nucl Med Mol Imaging. 2016;43:1929–30.
34. Giesel FL, Fiedler H, Stefanova M, Sterzing F, Rius M, Kopka K, et al. PSMA PET/CT with Glu-urea-Lys-(Ahx)-[68Ga(HBED-CC)] versus 3D CT volumetric lymph node assessment in recurrent prostate cancer. Eur J Nucl Med Mol Imaging. 2015;42:1794–800.
35. Eiber M, Weirich G, Holzapfel K, Souvatzoglou M, Haller B, Rauscher I, et al. Simultaneous 68Ga-PSMA HBED-CC PET/MRI Improves the Localization of Primary Prostate Cancer. Eur. Urol. [Internet]. 2016 [cited 2016 Sep 18]; Available from: http://linkinghub.elsevier.com/retrieve/pii/S0302283816000117
36. Rouvière O, Vitry T, Lyonnet D. Imaging of prostate cancer local recurrences: why and how? Eur Radiol. 2010;20:1254–66.